TECHNICAL PAPER

Experimental validation of the fluid–structure interaction simulation of a bioprosthetic aortic heart valve

I. Kemp · K. Dellimore · R. Rodriguez ·
C. Scheffer · D. Blaine · H. Weich ·
A. Doubell

Abstract Experiments performed on a 19 mm diameter bioprosthetic valve were used to successfully validate the fluid–structure interaction (FSI) simulation of an aortic valve at 72 bpm. The FSI simulation was initialized via a novel approach utilizing a Doppler sonogram of the experimentally tested valve. Using this approach very close quantitative agreement (≤ 12.5 %) between the numerical predictions and experimental values for several key valve performance parameters, including the peak systolic transvalvular pressure gradient, rapid valve opening time and rapid valve closing time, was obtained. The predicted valve leaflet kinematics during opening and closing were also in good agreement with the experimental measurements.

Keywords Aortic heart valve · Bioprosthetic valve · Fluid–structure interaction (FSI) simulation · Pulsatile flow

Abbreviations

BHV	Bioprosthetic heart valve
bpm	Beats per minute
CPD	Cardiac pulse duplicator
ET	Ejection time
FSI	Fluid–structure interaction
LDA	Laser Doppler anemometry
LFEL	Leaflet free edge length
PIV	Particle image velocimetry
rms	Root mean square
RVC	Rapid valve closing
RVCT	Rapid valve closing time
RVOT	Rapid valve opening time
STVPG	Systolic transvalvular pressure gradient
SVC	Slow valve closing

I. Kemp · K. Dellimore (✉) · R. Rodriguez · C. Scheffer ·
D. Blaine
Department of Mechanical and Mechatronic Engineering,
Stellenbosch University, Private Bag X1, Matieland,
Stellenbosch, Western Cape Province 7602, South Africa
e-mail: kiran.dellimore@gmail.com
URL: http://stbweb02.stb.sun.ac.za/berg/

H. Weich · A. Doubell
Division of Cardiology, Tygerberg Hospital and Stellenbosch
University, Private Bag X1, Tygerberg, Western Cape Province
7505, South Africa

Introduction

Aortic valve stenosis due to progressive calcification of aortic valve leaflets is one of the major causes of aortic valve disease in the geriatric population. It is the most frequent reason for prosthetic valve replacement in adults [1]. As a result over the past 50 years there has been significant research effort applied to the development of aortic valve prostheses, in particular bioprosthetic heart valves (BHVs) [2–7]. However, one of the major challenges in the BHV development process has been the availability of experimental flow and stress data to support the design of valve prostheses. Consequently, this has spurred interest in the numerical simulation of the behaviour of BHVs [8, 9]. With the rapid advancement in computational power, fluid–structure interaction (FSI) simulation has become an increasingly popular tool which is used to numerically model the performance of BHVs [9–26]. FSI simulations provide insight into the valve hemodynamics, the valve leaflet dynamics during opening and closing, as well as the stress experienced by the leaflets during valve operation. Research into the FSI modeling of native and prosthetic

aortic valves has been performed previously in two ways: through the coupling of computational fluid dynamics and finite element analysis software via user designed functions [10–12], or by using commercial FSI software packages [9, 13, 14]. However, among the many challenges involved in FSI modeling is the correlation and validation of numerical predictions with experimental measurements.

Numerous studies have attempted to validate FSI simulations of aortic heart valves using several different methods [9–26]. The most common approach used to validate the FSI simulations are the leaflet kinematics [9, 10, 14–16], visualisation of the fluid flow field using particle image velocimetry (PIV) [17–19] or laser Doppler anemometry (LDA) [20, 21], estimation of rapid valve opening, rapid valve closing and ejection times (RVOT, RVCT and ET, respectively) [22], and comparison of the simulated transvalvular pressure gradient waveform and velocity profile to experimental results [9, 10, 14, 22]. Hart et al. [20] and Dumont et al. [21] used LDA to validate the FSI simulation of a simplified model of a barrier (the leaflet) inside a box. Guivier-Curien et al. [18] and Falahatpisheh and Kheradvar [19] used PIV to validate FSI simulations of a bi-leaflet mechanical valve and mitral valve, respectively.

The aim of the current study is to present the experimental validation of the full, tri-leaflet FSI simulation of an aortic BHV using high speed imaging and Doppler echocardiography.

Materials and methods

Valve model

The test valve is a prototype tricuspid valve which is designed for transcatheter insertion and deployment through balloon expansion in the native aortic position [27–30]. The valve is supported on a 19 mm (inner diameter) electropolished L605 cobalt chrome stent, which measured 16 mm in height and had a wall thickness of 0.35 mm. The leaflets of the valve were made from pericardial kangaroo tissue treated with the ADAPT® process of Celxcel Pty Ltd. (an anticalcification process which is designed for glutaraldehyde-crosslinked tissues) and were attached to the stent with CV-7 (0.109 mm mean diameter and 0.40 kg knot-pull tensile strength) Gore-Tex© polytetrafluoroethylene suturing. Paravalvular leakage was prevented by enclosing the stent inside a 0.25 mm thick (single wall), biocompatible BARD polyester knit tube. The fibre alignment of the tissue used to make the leaflets was carefully chosen to lie in line with the circumferential direction of the valve to improve its strength. It was also found that one side of the kangaroo tissue was smooth while the other side possessed a fibrous surface texture. The smooth side of the tissue was chosen for sealing

between the leaflets, while the fibrous side was used for the inner part of the leaflet which comes into direct contact with the stent during valve operation. Complete details of the prosthetic valve fabrication process are reported by Esterhuyse [27, 28] and Smuts [29, 30], Aswegen [31, 32]. The final manufactured prosthetic valve is shown, in its relaxed state, in Fig. 1a. Table 1 summarizes the critical dimensions measured for each of the three leaflets. It is important to note that the twisting observed at the contact of the leaflets occurs due to the long free edge length used (21–22 mm).

Prior to fabrication of the valve, the pericardial kangaroo tissue was characterized using biaxial testing (to determine the stress–strain properties of the tissue) [29, 30] and histological testing (to determine the tissue thickness). These tests revealed that the tissue, with fibre alignment in the transverse direction, had a maximum normal stress value of 0.91 MPa at a strain value of 0.35. Also, since the histological tests indicated that the kangaroo tissue had a variable thickness, an average thickness (0.25 mm) was determined as reported in Table 1.

Experimental methods

A custom-built, cardiac pulse duplicator (CPD) system, which simulates the pumping action of the left ventricle of the heart, was used to perform the experimental analysis on the prosthetic aortic heart valve. A schematic diagram of the aortic flow valve chamber and a picture of the CPD system are shown in Fig. 2a. The design of the system was based on the four-element Windkessel model of the arterial system which uses a simple lumped parameter electrical analogy to simulate the total arterial impedance in the human body by accounting for the aortic and arterial resistance, arterial compliance, and blood inertance. The geometry of the aortic sinuses, coronary arteries and aortic arch were not included in the design of the CPD since the influence of these anatomical features on the flow waveforms in the aortic valve can be accounted for by varying the flow compliance, inertance and resistance; via opening or closing of the resistance valve and by changing the height of fluid in the compliance chamber to obtain physiologically appropriate conditions. Full details of the design and fabrication of the CPD are reported by Krynauw [33].

The CPD has four separate chambers for testing aortic valves at heart rates up to 250 bpm and is controlled with a LabView® graphical user interface. The working fluid in the CPD is a mixture of 48 % glycerol and 52 % saline solution (by mass), with 0.01 % sodium azide disinfectant, which has a similar density (1.05×10^3 kg m^{-3}) and viscosity (3.57×10^{-3} N s m^{-2}) to whole blood with a physiological hematocrit of 45 % at 37 °C [34]. A glycerol based blood analog was chosen for the working fluid in the CPD, since previous work by Carey and Herman [35] has

Fig. 1 **a** Photograph of the 19 mm diameter BHV used for the validation experiments. **b** Finite element model of the BHV. **c** Schematic of the 3-D finite element model and the relative boundary conditions
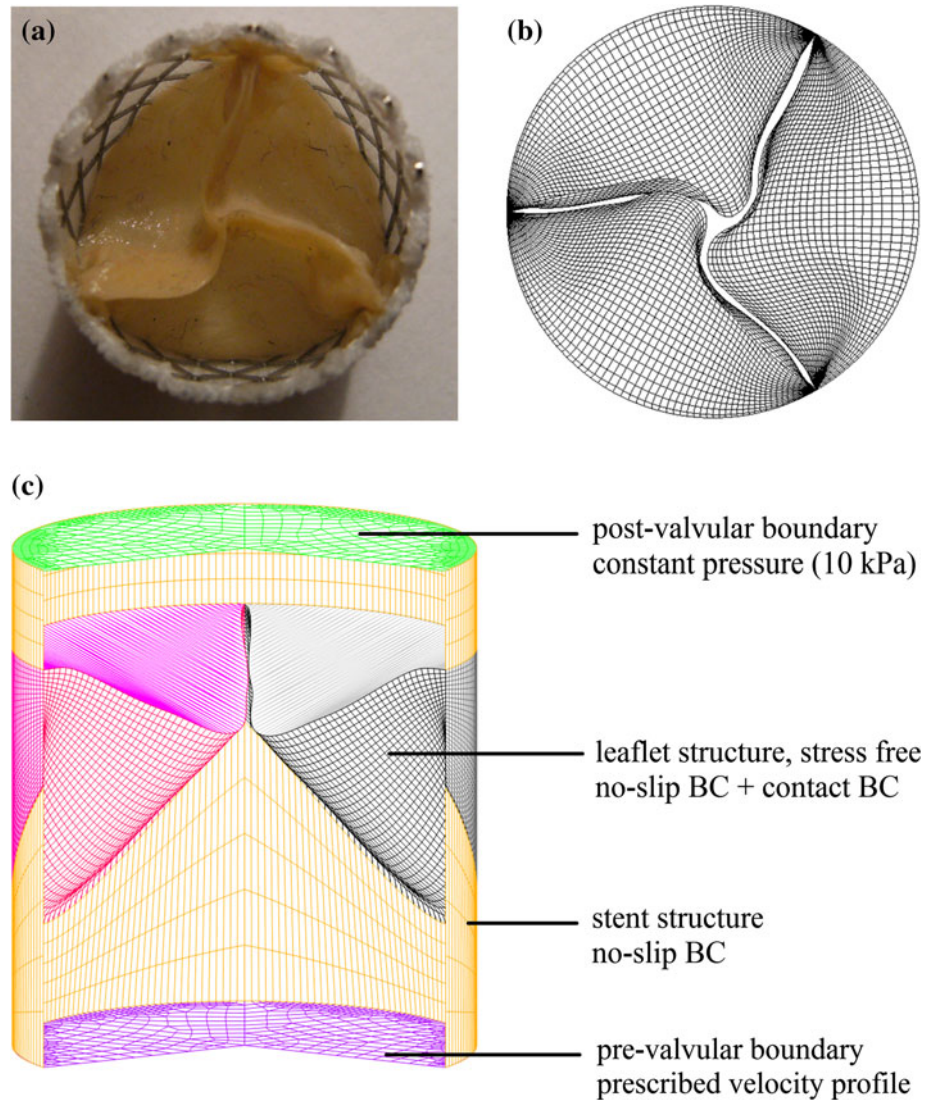

Post-valvular boundary constant pressure (10 kPa)

leaflet structure, stress free no-slip BC + contact BC

stent structure no-slip BC

pre-valvular boundary prescribed velocity profile

Table 1 Leaflet, stent and fluid properties used in the experiment and FSI simulations

Property	Value (units)
Leaflet free edge lengths[a]	22.0, 21.7, 21.2 (mm)
Leaflet heights[a]	13.6, 14.3, 14.2 (mm)
Heights of the leaflet commissures[a]	6.1, 6.1, 6.2 (mm)
Leaflet density	1.0×10^3 (kg m^{-3})
Leaflet elastic modulus	3.0×10^6 (N m^{-2})
Leaflet and stent Poisson's ratio	0.3 (–)
Average leaflet thickness	0.25 (mm)
Stent Elastic modulus	3.0×10^{11} (N m^{-2})
Stent density	7.85×10^3 (kg m^{-3})
Stent height	16.0 (mm)
Fluid density	1.05×10^3 (kg m^{-3})
Fluid dynamic viscosity	3.57×10^{-3} (N s^{-1} m^{-2})

[a] Dimensions are given for leaflet 1, 2 and 3 (in that order)

shown that glycerol absorption does not adversely affect leaflet stiffness or mechanical performance. Nevertheless, as a precaution against dehydration, prior to commencing each test the prototype and control valves were hydrated in saline solution for 10 min and all valve tests were restricted to a maximum duration of 6 h. The mixture was heated using two submersible RS Components 300 W heaters with a network of five HT model HJ-541 pumps to ensure that the mixture was at a uniform temperature. The mixture temperature was maintained at 37 °C using a Delta DTA PID controller with an RTD PT100 sensor which is capable of regulating the mixture temperature to within 0.2 °C.

Valve flow characterization

The pre-valvular and post-valvular pressure measurements were recorded using two WIKA model A-10 pressure transducers mounted on the ventricular and aortic side of
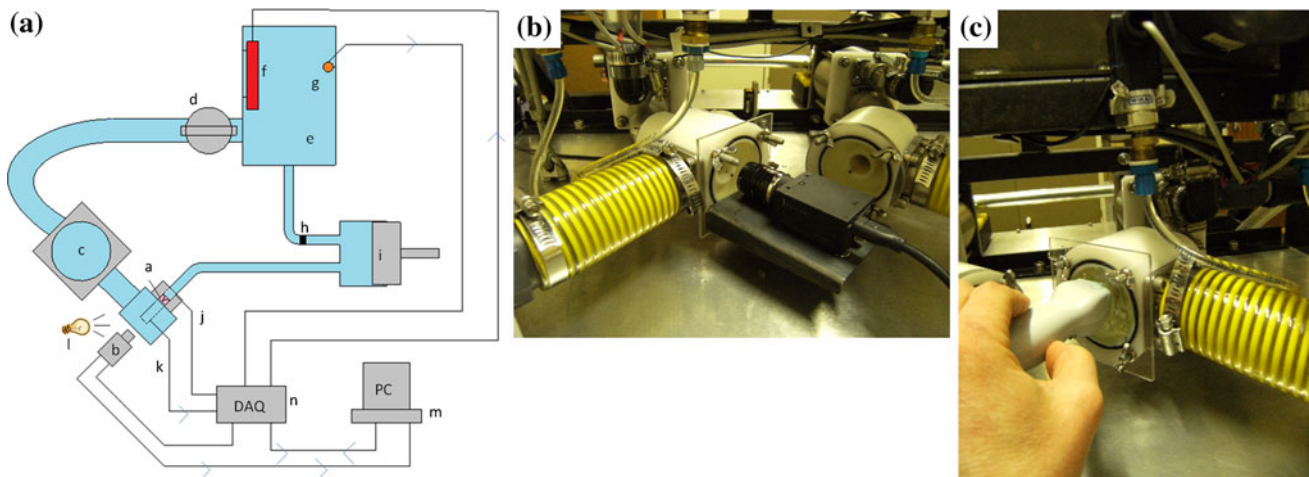
Fig. 2 a Schematic of one line on the CPD. *a* valve prosthesis, *b* camera, *c* compliance chamber, *d* ball valve (resistance valve), *e* fluid tank, *f* heater element, *g* temperature sensor, *h* mitral valve, *i* piston, *j* pre-valvular pressure line, *k* post-valvular pressure line, *l* light source, *m* computational station, *n* digital acquisition unit. **b** Experimental setup for: imaging with the high speed camera and **c** Doppler echocardiography

the valve test chamber. The transvalvular pressure gradient was determined from these measurements by subtracting the post-valvular pressure from the pre-valvular pressure. Images of the BHV were acquired using a 0.3 Megapixel Grasshopper GRAS-03K2 M-C digital camera (Fig. 2b). A triggering system controlled via a LabVIEW® program was used to synchronize the pressure transducer measurements with the acquisition of images from the high speed camera. Images were acquired with the camera mounted on a platform attached to the base of the valve chamber with the lens situated 1.1 cm from the valve chamber window and 8.0 cm from the valve. The average frame rate during acquisition at 72 bpm was 288.2 fps over a period of 5.2 s, which corresponded to six consecutive cardiac cycles. The systolic phase of each cycle was compared to ensure that there were no significant differences between the opening and closing behaviour of the leaflets.

A SonoSite™ MicroMaxx array system using a 25 mm, 1–5 MHz, independent P17 phased array Doppler imaging transducer (probe) (Fig. 2c), capable of operating in continuous and pulsed wave modes was used to take the Doppler echocardiographic measurements. The following parameters were used for all readings: fractional echo readout using 70–100 % of the full echo; Doppler angle, 0°; bandwidth, in the range of 5.2–41.7 kHz, velocity sensitivity, 200 cm s^{-1} along all 3 spatial directions; fractional field of view, (300–340 × 225–240) mm^2; slab thickness, 83.2–96 mm; matrix, 256 × 144 × 32; and spatial resolution, (1.17–1.33 × 1.56–1.67 × 2.60–3.00) mm^3. The peak flow velocity was measured by placing the probe in-line with the flow through the prosthesis in contact with the window of the valve chamber (Fig. 2c). The Doppler transmit beam was placed as perpendicular as possible to the plane of the valve ring, with very slight angulation of the

probe required to obtain the maximal flow velocity. It was not possible to acquire velocity data at the same time as the images because both measurement methods required access to the front of the viewing window. The high speed imaging tests were therefore performed first, followed by the Doppler echocardiographic measurements which were taken under identical conditions.

Numerical approach

FSI simulations of the full, tri-leaflet prosthetic valve, during systole, were performed using the commercial software MSC.Dytran. An explicit finite element approach was used to solve the governing equation of motion for the structure [36]:

$$F_n^{\text{ext}} = Ma_n + Cv_n + Kd_n \quad (1)$$

where *M*, *C* and *K* are the mass, damping and stiffness matrices of the system, respectively, a_n, v_n and d_n are the acceleration, velocity and displacement at the current time step *n*, respectively and F_n^{ext} is the vector of externally applied loads. A Reimann-based, explicit Euler method was used to solve the governing fluid mass and momentum equations:

$$\frac{\partial \rho}{\partial t} + \frac{\rho \partial(u_i)}{\partial x_i} = 0 \quad (2)$$

$$\begin{aligned}&\frac{\rho \partial(u_i)}{\partial t} + \frac{\rho \partial(u_i u_j)}{\partial x_j} + \frac{\partial p}{\partial x_i} - f_i \\&- \mu \frac{\partial}{\partial x_j}\left(\frac{\partial u_i}{\partial x_j} + \frac{\partial u_j}{\partial x_i} - \frac{2}{3}\delta_{ij}\frac{\partial u_l}{\partial x_l}\right) \\&= 0\end{aligned} \quad (3)$$

where *x* is the spatial displacement, ρ is the fluid density, *p* is the pressure, *u* is the fluid velocity, *t* is the time, *f* is the vector of body forces, μ is the viscosity and δ_{ij} is the

Kronecker delta stress tensor. The system of equations is closed by solving the simple bulk modulus (K_{bulk}) fluid equation of state:

$$p = K_{bulk} \left(\frac{\rho}{\rho_0} - 1 \right) \tag{4}$$

where ρ_0 is the fluid reference density.

A global damping coefficient, called *vdamping*, was introduced into the simulations. This was necessary to keep the solution from becoming unstable. This damping coefficient is based on a mass–spring–damper system and is related to the natural frequency of the entire system, ω. It is applied to the equation of motion by factoring the velocity, v_i, at every time step as follows:

$$v_i^{n+1/2} = \frac{1-\omega}{1+\omega} v_i^{n+1/2} + \frac{\Delta t}{1+\omega} \left\{ \frac{f_{ext}^n - f_{int}^n}{m_i} \right\} \tag{5}$$

where f_{ext}^n and f_{int}^n are the external and internal forces acting on the body at the current time step and m is the mass of the body.

In order to minimize interference with the numerical solution path a *vdamping* value of 0.003 was used.

Finite element valve model and materials

The FE valve model was created based on the geometry of the experimentally tested BHV. Figure 1b is a top view of the finite element model of the leaflets in the closed, stress free (diastolic) position while Fig. 1c is the schematic of the valve model showing the boundary conditions. Due to the complexity of the experimental setup a number of simplifications and assumptions were made for the simulations. The FE model consisted of a straight rigid outer cylinder with the leaflets situated in the middle of the cylinder; the base of the valve and top of the commissures located 5 mm from the inflow and outflow surfaces,

respectively. The leaflets consisted of 1.91×10^3 quadrilateral Keyhoff shell elements. The FE model consisted of over 1.60×10^4 elements while the Euler domain consisted of 1.70×10^5 finite volume brick elements. A grid independence test, using a one-third model of the valve, revealed that this mesh size was sufficient to resolve the flow through the valve (Fig. 3a, b). During these tests the flow conditions were kept constant for all the simulations and only the number of finite volume brick elements was changed. The peak velocity was recorded along the model centreline for each of the cases as well as the rapid valve opening time (RVOT) and rapid valve closing time (RVCT).

The material properties of the valve leaflets were specified based on the mechanical properties of the leaflets of the BHV which were measured prior to fabrication (Table 1). The leaflet material was modeled as a linear isotropic material (since the valve experiences very little strain during systole) with a thickness of 0.25 mm (based on the average tissue thickness determined from histological testing, since the kangaroo tissue used to make the test valve had a variable thickness), and an elastic modulus of 3 MPa. The fluid flow in the valve was modeled as incompressible and laminar, while the fluid density and dynamic viscosity were prescribed to match the experimental conditions. Also, the fluid was assumed to be Newtonian, which is consistent with several previous heart valve simulation studies [9, 12, 15, 16, 37].

Boundary conditions, initialization and solution method

The flow through the valve was driven using a transient velocity curve derived from the Doppler echocardiographic image (Fig. 4a), of one 72 bpm cycle, from the experiment. No-slip boundary conditions were applied to the leaflet and
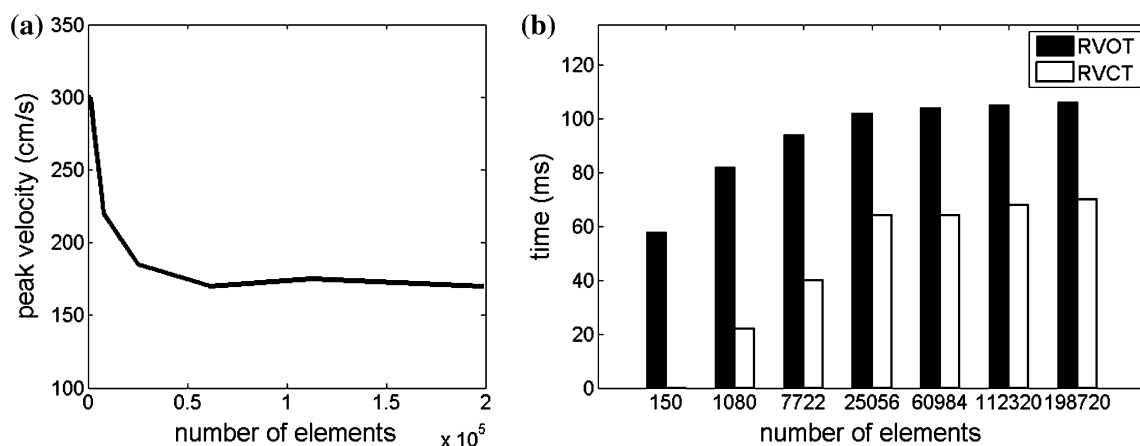

Fig. 3 Grid independence tests results. **a** Predicted peak centreline velocity through the valve as a function of the number of finite volume brick elements. **b** Predicted RVOT and RVCT as a function of the number of finite volume brick elements
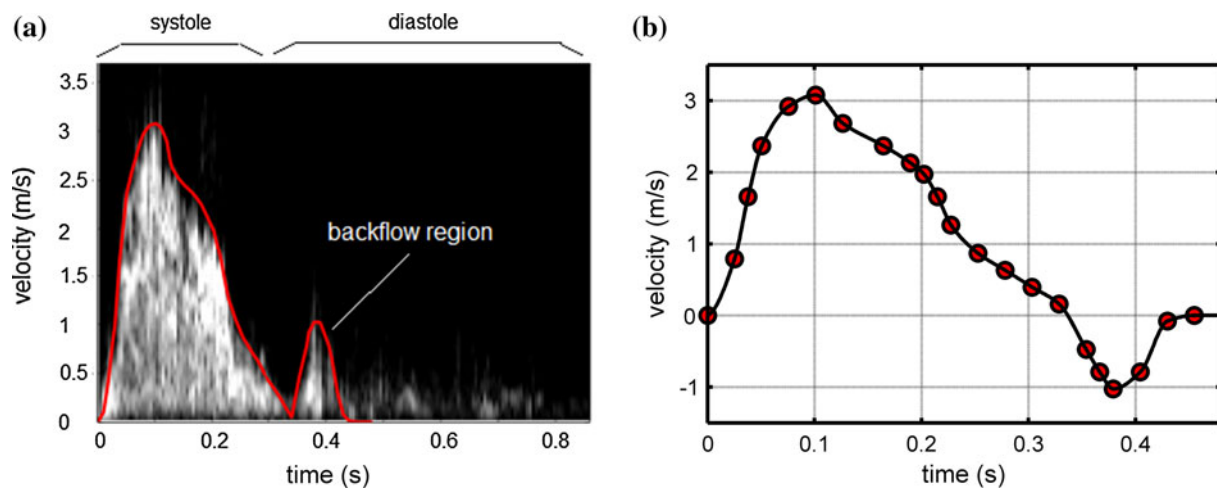
Fig. 4 a Transient velocity Doppler echocardiograph image. **b** Velocity profile obtained from an 8th order polynomial fit of the Doppler velocity data which was specified at the inflow (pre-valvular) boundary of the FSI simulation

Table 2 Summary of the average ET, RVOT, RVCT, and STVPG measured during the experiment and predicted by the FSI simulation for the 19 mm BHV

	RVOT (ms)	RVCT (ms)	ET (ms)	Peak STVPG (mmHg)
Experiment	37.0 ± 3.1	77.1 ± 5.8	366.8 ± 2.0	26.7
FSI simulation	40.0	88.0	378.0	23.36
Relative difference (%)	7.5	12.4	3.0	12.5

RVOT Rapid valve opening time, the time from when valve opening was initiated until the valve was fully open; *RVCT* rapid valve closing time, the time from when rapid valve closing was initiated until the valve was fully closed; *ET* ejection time, the time taken from the initial opening to complete closure of the valve, and *STVPG* systolic transvalvular pressure gradient, the maximum pressure difference across the valve during systole

stent structure surface elements. The valve model has two master–slave-node contact boundary conditions applied to the leaflet and stent structure. All Euler elements were initialized to a pressure of 10 kPa with zero stress present. A no stress boundary condition was also applied to all Lagrangian elements. The fluid boundary conditions consist of an inflow (pre-valvular), an outflow (post-valvular) and a no slip boundary. The inflow velocity was prescribed from the Doppler measurements (Fig. 4a) by sampling the Doppler image at discrete points, which were then fitted with an 8th order polynomial in order to obtain a smooth velocity profile (Fig. 4b). At the outflow boundary a constant 10 kPa boundary condition was applied. MSC.Dytran's general fast coupling algorithm was used to link the structural and fluidic solvers [36]. The numerical simulations were performed on the Stellenbosch University High Performance Computer

Cluster using four central processing units on a single node and were completed in ~ 250 h.

Data analysis and post-processing

The results of the numerical simulations were post-processed using Ensight 8.2 and MSC.Patran to gain insights into valve hemodynamics, the valve leaflet dynamics during opening and closing, as well as the stress experienced by the leaflets during valve operation. The RVOT was calculated from the time taken for the valve to go from a closed to a fully open position. The RVCT was computed from the time when the valve started to close until it was completely closed. The ET was found by computing the time taken from the initial opening to complete closure of the valve. All values for the RVOT, RVCT and ET reported in Table 2 for the experiment were obtained by averaging over several cardiac cycles and are reported as mean $\pm$ S.D. The peak systolic transvalvular pressure gradient (STVPG) was computed by finding the difference between the aortic and ventricular pressures during systole. The experimental values for the RVOT, RVCT, ET and STVPG are based on the average of five recorded cycles. The relative difference was computed as the ratio of the difference between the simulation result and the experimental result, to the simulation result. The average root mean square (rms) error was calculated as the square root of the sum of the squared difference terms between the simulation and experimental results per sample divided by the sum of the total number of samples:

$$RMS\,error = \sqrt{\frac{\sum_{i=1}^{n} (\hat{y}_i - y_i)^2}{n}} \qquad (6)$$

where n is the number of samples, $\hat{y}_i$ and y_i are the experimental and simulation results, respectively, at sample i.
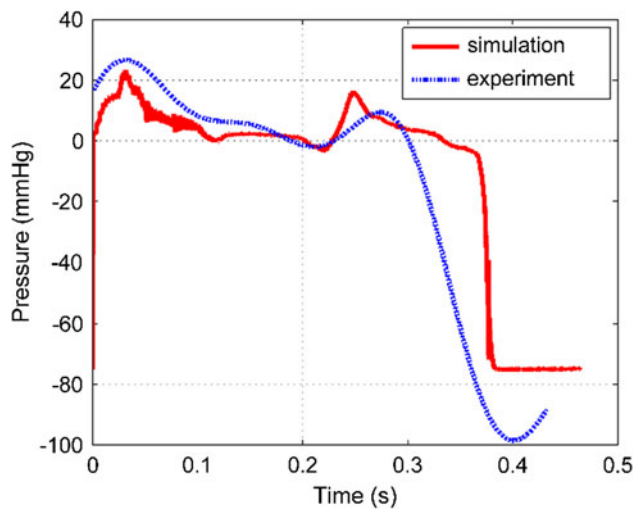
Fig. 5 Comparison of the experimental and simulated transvalvular pressure gradient

Results

Valve hemodynamics

Figure 5 shows the transvalvular pressure comparison between the experimental and simulated results. The solid line corresponds to the FSI simulation predictions and the dash-dot line to the experimental measurements. The experimental and numerically predicted transvalvular pressure gradients correspond to the time at which the initiation of leaflet opening occurs. The experimental and simulated STVPG occur at similar times during the first 0.05 s of systole (i.e., 0.031 and 0.032 s, respectively). The peak STVPG predicted by the FSI simulations was 23.36 mmHg while for the experiment it was 26.7 mmHg, which corresponds to a relative difference of 12.5 % (It is important to note here that this difference is computed based on a comparison of the numerical results with the average of all of the experimental data).

Valve kinematics

Figure 6 compares the opening and closing images of the experimental and simulated valve. The time (in ms) at which each image was taken is written in the upper left corner of the respective images. The valve opening images (Fig. 6a) are arranged in ascending order of time from the start of leaflet opening until the leaflets are fully open. The closing of the valve is shown in Fig. 6b, with the images arranged in ascending order of time from the point at which leaflet closing was initiated until the complete closure of the leaflets. For the 72 bpm cardiac cycle shown, the experimental ET was 363.7 ms, the RVOT was 40.8 ms
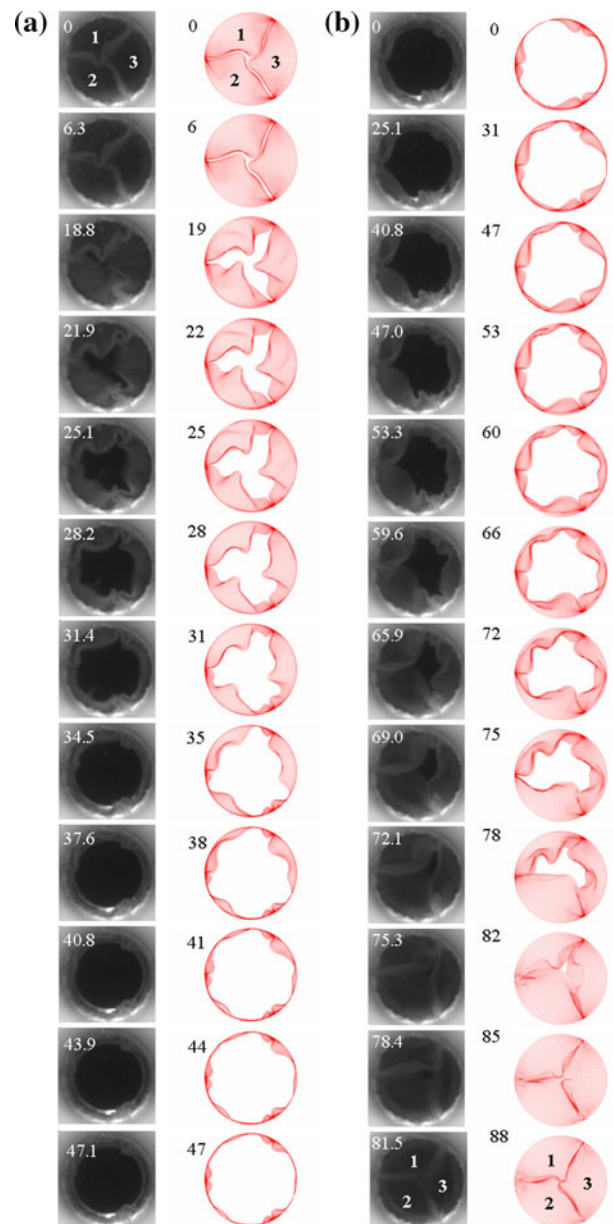

Fig. 6 Comparison of the experimental and numerically predicted BHV leaflet dynamics during: **a** opening and **b** closing

and the RVCT was 81.5 ms. The numerically predicted ET, RVOT and RVCT agreed with the averaged experimental results to within a relative difference of 3.0, 7.5 and 12.4 %, respectively (Table 2).

Leaflet stress distribution

Figure 7 shows the Von Mises stress distribution in the leaflets when the valve is open and when the valve is closed. The peak Von Mises stress for the open position occurs at the tip of the leaflet with a magnitude of 0.5 MPa, indicated in Fig. 7, while in the closed position it occurs at

Fig. 7 Contours of BHV leaflet stresses in the: (a) open and (b) closed positions
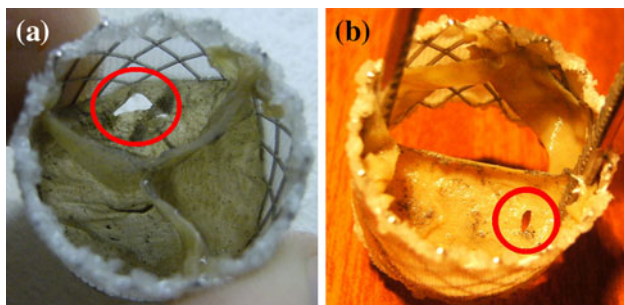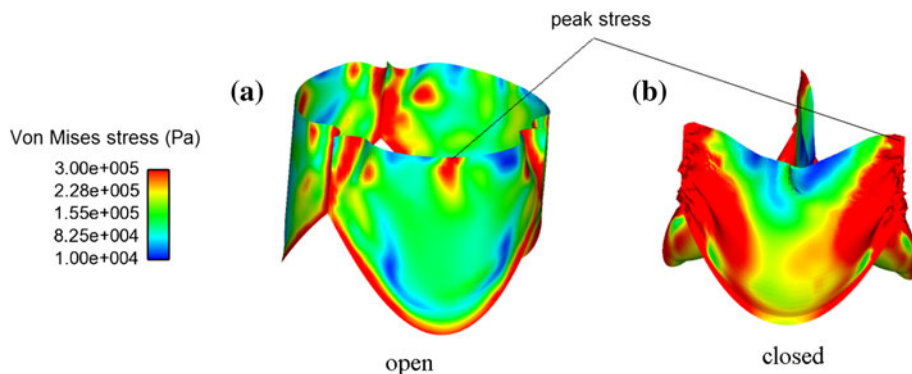

Fig. 8 Photographs showing BHV leaflet damage

the top of the commissures with a magnitude of 1.23 MPa, as indicated in Fig. 7.

Figure 8a, b show the damage to the valve leaflets after exposing two valves to arrhythmic heart rates of up to 200 bpm and diastolic pressures up to 500 mmHg. The damage is due to tearing and not fatigue of the leaflets. The leaflets were torn on the side (Fig. 8b), close to the commissure edge, and at the central basal area (Fig. 8a) (the central region of the leaflet), close to the base of the leaflet attachment. This indicates that the leaflets experience the greatest stress close to the commissures and at the central basal area of the leaflet during diastole.

Discussion

The transient transvalvular pressure waveforms plotted in Fig. 5 for the experiment and FSI simulation show that the pressure initially rises during leaflet opening, due to the rapid acceleration of the flow through the valve at the beginning of systole, until it reaches the peak STVPG. This peak pressure occurs at roughly the same time (31 ms) in each case and corresponds to the time at which the valve is almost fully open. Thereafter the pressure decreases to a physiologically normal STVPG of between 2 and 7 mmHg, since the flow is no longer obstructed by the leaflets. The pressure then dips below zero for a short period of time before rising to a second peak, which is lower than the

maximum STVPG. This is then followed by a period of very gradual decrease in pressure in which the valve begins to close. After that the valve closes very rapidly, as indicated by the sudden decrease in pressure, until the diastolic transvalvular pressure is reached and the valve is completely closed.

Comparison of the FSI predictions and the experimental measurements in Fig. 5 shows that the transvalvular pressure predicted numerically remains lower than in the experiment during the first half of systole, while during the second half of systole it is higher. In spite of these differences, both curves follow the same trends over almost the entire systolic phase. The average rms error between the experiment and simulation predictions for the STVPG is 51.3 mmHg over the entire systolic phase, but it is only 13.8 mmHg over the first 80 % of systole. A major source of this error can be attributed to the noise in the FSI predictions which occurs due to the fairly coarse velocity profile specified at the inflow boundary and because of the fact that the experimental valve closes slightly earlier than the numerically modelled valve. This latter reason is significant because there is an 11.2 ms difference between the measured and predicted ETs of 366.8 and 378.0 ms, respectively (Table 2).

Figure 6 shows the kinematic opening and closing comparison between the experimental and numerically simulated valve. The valve opens relatively symmetrically in both the experiment and the FSI simulation as seen in Fig. 6a. At the start of rapid valve opening the leaflets are twisted about the axial plane due to the leaflet free edge length (LFEL) being longer than ideal. For leaflets with an ideal LFEL, the middle of the free edge would meet at the centre of the valve and open smoothly with low energy expenditure. The longer LFEL introduces a small amount of asymmetry into the opening of the leaflets. This is observed in both the experiment and the FSI simulation predictions. However, the simulated valve takes 3 ms longer to fully open when compared to the experimental valve.

During valve closing shown in Fig. 6b there is a period of slow valve closing (SVC) followed by rapid valve

closing (RVC). This makes determining the start of RVC somewhat challenging and ambiguous. In both the experimental results and numerical predictions the closing of the valve is highly asymmetrical. The asymmetry in the closing of the simulated valve is likely attributable to the difference in the leaflet dimensions, leaflet interaction and to the different Euler domains for each leaflet. Both the experiment and FSI simulation show that leaflet 1 and 2 close quicker than leaflet 3 (Fig. 6b) which indicates that they extend further than leaflet 3 in order to close. This places greater strain on the leaflets 1 and 2, which may lead to leaflet fatigue damage and failure much sooner than in leaflet 3. Once the leaflets have closed, the flow is stopped and the point at which the leaflets meet is displaced back to the centre of the valve in a twisted position. The RVOT was determined from the time at which valve opening was initiated until the valve was fully open. The RVCT was determined as the time from when RVC was initiated to when the valve was fully closed [14]. The ET was determined from the time interval between the initiation of opening and complete closure of the valve. The results presented in Table 2 indicate that the RVOT, RVCT and ET of the simulated valve correlate well with the average experimental values, within relative differences of 7.5, 12.4 and 3.0 %, respectively. These margins of error are reasonable and indicate that the FSI simulations are able to accurately predict the behaviour of the valve leaflets during systole. As noted previously, a likely major source for the discrepancies between the numerical predictions and experimental measurements is the coarseness of the input velocity profile for the FSI simulations. Further simulations indicated that a slight variation in the velocity profile had a significant influence on the valve dynamics, particularly during closure [38].

The images of the leaflet Von Mises stress in the open and closed position, shown in Fig. 7, provide insight into the areas of the valve leaflets that are most likely to fail. The stress patterns indicate that the maximum stress occurs along the suture line when the leaflets are fully open during systole and close to the commissures, extending towards the central basal area of the leaflet during diastole. The FSI predictions are consistent with experimental observations of leaflet damage which occurred in one of the test valves, which is shown in Fig. 8. Figure 8a image shows a tear at the central basal area of the leaflet while Fig. 8b shows a tear close to the commissures. While it is important to note that this leaflet damage occurred at an elevated pressure and at an arrhythmic heart rate (200 bpm), which correspond to a harsher environment than expected under normal physiological conditions, this result is still useful since these extreme conditions allow the mechanically weaker areas of the valve leaflets (which are most likely fail during normal valve operation) to be more easily identified.

Moreover, the valve damage observed in Fig. 8a, b is consistent with the type of leaflet failure described by Sun et al. [39]. The tearing of the tissue can be attributed to the high back pressure during diastole which causes large forces to be exerted on the areas of the leaflets that experience the highest stress (see labelled regions in Fig. 7), which over many repeated cycles leads to ripping of the tissue in these locations. This result suggests that the FSI simulations are able to correctly predict the areas of the valve leaflets that are likely to suffer damage or failure during long term valve operation.

The results presented in this study are subject to the following limitations. Firstly, due to physical limitations of the CPD it was not possible to measure the flow velocity and leaflet kinematics of the test valve simultaneously. Although every effort was made to match the conditions between tests there may still have been minor differences between the conditions during high speed imaging and Doppler echocardiography. Secondly, the test valve was fabricated by hand. This may have introduced slight defects, such as over-sizing of the LFEL and uneven suturing. These defects could not be replicated in the numerical model and also may have introduced additional asymmetric behaviour in the experimental test valve. Thirdly, the FSI simulation was limited by the available material model used for the leaflets and the coarseness of the velocity profile prescribed at the inflow boundary based on the experimental Doppler echocardiographic measurements. In the former case, the leaflet tissue used to make the experimental test valve has non-linear anisotropic material properties. However, due to difficulties in implementing a non-linear material model, a linear isotropic model was used instead. In the latter case, the coarse (i.e., not smooth) input velocity profile for the FSI simulations introduced a small amount of noise in the numerical predictions which may have contributed to the mismatch between simulation and experiment. Fourthly, the FSI simulations relates to the use of a damping factor in order to avoid distortion of the Lagrangian elements in the computational model of the valve. This may have introduced minor numerical errors into the simulation such as decreased grid point velocities, which may have caused slower closing of the valve leaflets. Fifthly, it is also important to point out that the stress values presented in Fig. 7 have not been validated against numerical data and therefore can only provide a relative indication of the stress distribution in the leaflets of the valve. Another limitation in this study is the fact that the FSI simulations of the BHV have only been validated against experimental data at a single heart rate (72 bpm) and therefore the conclusions should be carefully interpreted with respect to higher or lower heart rates. Lastly, the velocity profile specified at the inflow boundary had a peak velocity of 309 cm s^{-1}

which corresponds to a mild degree of stenosis. This high velocity can be attributed to two main factors. First, the diameter of the prototype valve (19 mm) is smaller than that of a typical native human aortic valve (about 23 mm) which means that for the same cardiac output the average velocity of the flow will be 46.5 % higher, based on mass conservation. Second, the cardiac output was 7.0 L min^{-1}, which is slightly higher than in normal human adults (5.0–6.0 L min^{-1}).

Conclusions

CPD experiments performed on a 19 mm diameter bio-prosthetic valve were used to successfully validate the FSI simulation of an aortic valve at 72 bpm. The FSI simulation was initialized via a novel approach utilizing a Doppler sonogram of the experimentally tested valve. Using this approach very close quantitative agreement (≤12.5 %) between the numerical predictions and experimental values for several key valve performance parameters, including the peak STVPG, RVOT and RVCT, was obtained. The predicted leaflet kinematics during opening and closing were also in good agreement with the experimental measurements.

References

1. Flachskampf FA, Daniel WG (2004) Aortic valve stenosis. Internist (Berl.) 45(11):1281–1290
2. Wong C, Shital P, Chen R, Owida A, Morsi Y (2010) Biomimetic electrospun gelatinchitosan polyurethane for heart valve leaflets. J Mech Med Biol 10(4):563–576
3. Morsi YS (2012) Tissue engineering of the aortic heart valve: fundamentals and developments. Nova Science Publishers, New York
4. Patel SS, Morsi, YS (2010) Making of functional tissue engineered heart valve. IFMBE Proceedings 32:180–182
5. Morsi YS, Wong CS (2008) Current developments and future challenges for the creation of aortic heart valve. J Mech Med Biol 8(1):1–15
6. Morsi YS, Birchall I (2005) Tissue engineering a functional aortic heart valve: an appraisal. Future Cardiol 1(3):405–411
7. Morsi YS, Birchall IE, Rosenfeldt FL (2004) Artificial aortic valves: an overview. Int J Artif Organs 27(6):445–451
8. Morsi Y, Ahmad A, Hassan A (2001) Numerical simulation of the turbulent flow field distal to an aortic heart valve. Front Med Biol Eng 11(1):1–11
9. Carmody CJ, Burriesci G, Howard IC, Patterson EA (2006) An approach to the simulation of fluid–structure interaction in the aortic valve. J Biomech 39(1):158–169
10. Griffith BE (2012) Immersed boundary model of aortic heart valve dynamics with physiological driving and loading conditions. Int J Numer Method Biomed Eng 28(3):317–345
11. Nobili M, Morbiducci U, Ponzini R, del Gaudio C, Balducci A, Grigioni M, Montevecchi FM, Redaelli A (2008) Numerical simulation of the dynamics of a bileaflet prosthetic heart valve using a fluid–structure interaction approach. J Biomech 41(11): 2539–2550
12. Van Loon R, Anderson PD, de Hart J, Baaijens FPT (2004) A combined fictitious domain/adaptive meshing method for fluid–structure interaction in heart valves. Int J Numer Method Fluids 46(5): 533–544
13. Becker W, Rowson J, Oakley JE, Yoxall A, Manson G, Worden K (2011) Bayesian sensitivity analysis of a model of the aortic valve. J Biomech 44(8):1499–1506
14. Ranga A, Bouchot O, Mongrain R, Ugolini P, Cartier R (2006) Computational simulations of the aortic valve validated by imaging data: evaluation of valve-sparing techniques. Interact Cardiovasc Thorac Surg, 5:373–378
15. De Hart J, Peters GW, Schreurs PJ, Baaijens FP (2003) A three-dimensional computational analysis of fluid–structure interaction in the aortic valve. J Biomech 36(1):103–112
16. Van Loon R 2005 A 3D method for modelling the fluid–structure interaction of heart valves. PhD Dissertation, Technische Universiteit Eindhoven
17. Dasi, LP, Ge, L, Simon, HA, Sotiropoulos, F, and Yoganathan, AP (2007) Vorticity dynamics of a bileaflet mechanical heart valve in an axisymmetric aorta. Phys Fluids 19(6):067105
18. Guivier-Curien C, Deplano V, Bertrand E (2009) Validation of a numerical 3-D fluid–structure interaction model for a prosthetic valve based on experimental PIV measurements. Med Eng Phys 31:986–993
19. Falahatpisheh A, Kheradvar A (2012) High-speed particle image velocimetry to assess cardiac fluid dynamics in vitro: from performance to validation. Eur J Mech B-Fluid 35:2–8
20. De Hart J, Peters GW, Schreurs PJ, Baaijens FP (2000) A two-dimensional fluid–structure interaction model of the aortic valve. J Biomech 33:1079–1088
21. Dumont, K, Stijnen JM, Vierendeels J, van de Vosse FN, Verdonck PR (2004) Validation of a fluid–structure interaction model of a heart valve using the dynamic mesh method in fluent. Comput Methods Biomech Biomed Eng 7(3):139–146
22. Weinberg E, Mofrad M (2007) Transient, three-dimensional, multiscale simulations of the human aortic valve. Cardiovasc Eng 7(4):140–155
23. Borazjani I, Ge L, Sotiropoulos F (2010) High-resolution fluid–structure interaction simulations of flow through a bi-leaflet mechanical heart valve in an anatomic aorta. Ann Biomed Eng 38(2):326–344
24. Marom G, Haj-Ali R, Raanani E, Schäfers HJ, Rosenfeld MA (2012) A fluid–structure interaction model of the aortic valve with coaptation and compliant aortic root. Med Biol Eng Comput 50(2):173–182
25. Chandra S, Rajamannan NM, Sucosky P (2012) Computational assessment of bicuspid aortic valve wall-shear stress: implications for calcific aortic valve disease. Biomech Model Mechanobiol 11:1085–1096
26. Kouhi E, Morsi Y (2010) Fluid–structure interaction analysis of stentless bio-prosthetic aortic heart valve in the sinus of valsalva. ASME IMECE Proceedings 2:789–798
27. Esterhuyse A (2009) Structural design of a stent for a percutaneous aortic heart valve. MSc Thesis, Stellenbosch University
28. Esterhuyse A, van der Westhuizen K, Doubell A, Weich H, Scheffer C, Dellimore K (2012) Application of the finite element method to the fatigue life prediction of a stent for a percutaneous heart valve. J Mech Med Biol 12(1):1–18

29. Smuts AN (2009) Design of tissue leaflets for a percutaneous aortic valve. MSc Thesis, Stellenbosch University

30. Smuts AN, Blaine DC, Scheffer C, Weich H, Doubell AF, Dellimore KH (2011) Application of finite element analysis to the design of tissue leaflets for a percutaneous aortic valve. J Mech Behav Biomed Mater 4(1): 85–98

31. Van Aswegen K (2008) Dynamic modelling of a stented aortic valve. MSc Thesis, Stellenbosch University

32. Van Aswegen KHJ, Smuts AN, Scheffer C, Weich HSV, Doubell AF (2012) Investigation of leaflet geometry in a percutaneous aortic valve with the use of fluid–structure interaction simulation. J Mech Med Biol 12(1):1–15

33. Krynauw H (2009) Design and implementation of an apparatus for hydrodynamic and fatigue testing of prosthetic aortic valves. MSc Thesis, University of Cape Town

34. Sherwood L (2008) Human physiology: from cells to systems. Brooks Cole, Belmont

35. Carey RF, Herman BA (1989) The effects of a glycerin-based blood analog on the testing of bioprosthetic heart valves. J Biomech 22:1185–1192

36. MSC.Software Corporation (2010) Dytran Theory Manual

37. Morsi YS, Yang WW, Wong CS, Das S (2007) Transient fluid–structure coupling for simulation of a trileaflet heart valve using weak coupling. J Artif Organs 10:96–103

38. Kemp IH (2012) Development, testing and fluid–structure interaction simulation of a bioprosthetic valve for transcatheter aortic valve implantation. MSc Thesis, Stellenbosch University

39. Sun W, Abad A, Sacks MS (2005) Simulated bioprosthetic heart valve deformation under quasi-static loading. J Biomech Eng 127(6):905–914